Available online at www.sciencedirect.com
ScienceDirect
Earth and Planetary Science Letters 256 (2007) 244–257
EPSL
www.elsevier.com/locate/epsl

High-precision U–Pb zircon age constraints on the Carboniferous–Permian boundary in the southern Urals stratotype

Jahandar Ramezani [a], Mark D. Schmitz [b,*], Vladimir I. Davydov [b], Samuel A. Bowring [a], Walter S. Snyder [b], Clyde J. Northrup [b]

[a] Department of Earth, Atmospheric and Planetary Sciences, Massachusetts Institute of Technology, Cambridge, Massachusetts 02139, USA
[b] Department of Geosciences, Boise State University, Boise, Idaho 83702, USA

Received 25 July 2006; received in revised form 27 January 2007; accepted 29 January 2007
Available online 3 February 2007
Edited by: R.W. Carlson

Abstract

Volcanic-ash beds within fossiliferous strata of the southern Uralian foredeep of Russia have been dated by the high-precision ID-TIMS U–Pb zircon method, to constrain the age of the Carboniferous–Permian transition. The stratigraphic section exposed at the Usolka locality, an auxiliary stratotype for the Carboniferous–Permian boundary, contains a detailed multi-taxa biostratigraphy with a well-resolved boundary succession tied to the Global Stratotype Section and Point (GSSP) at Aidaralash Creek (Kazakhstan). Four tuffs bracketing the Carboniferous–Permian transition in the Usolka section closely constrain the age of the boundary to 298.90+0.31/−0.15 Ma (2σ), including both analytical and stratigraphic uncertainty. These data substantially improve the calibration of the geologic time scale in the Late Paleozoic, and presage the radiometric age resolution possible for the late Carboniferous and early Permian stages through continued analysis of ash beds in the southern Urals stratotypes. By stabilizing the numeric age for the base of the Permian, these data also provide an important link between the timing of Permo-Carboniferous glaciation in Gondwana and its far-field climatic and sedimentological consequences in Euramerica.

Keywords: Carboniferous; Permian; boundary; U–Pb; Zircon; Ural Mountains

1. Introduction

The geologic time scale is a fundamental tool in Earth sciences research — the global correlation of events and the calculation of rates of geological and biological processes during Earth's history depend directly on the accuracy and precision of the geologic time scale. Yet despite its critical role, the numerical calibration of significant intervals of the time scale remains poor due to a lack of accurate, high-precision radiometric ages tied to high-resolution biostratigraphic contexts. The Late Paleozoic provides an important example: commonly cited time scales differ by as much as 10 Ma in the estimated age of the Carboniferous–Permian (C–P) boundary, and vary by as much as 500% in the inferred duration of various stages [1–5]. Without a precisely calibrated Pennsylvanian and Permian time scale, basic questions regarding the final assembly and early evolution of Pangaea, the paleoclimatic transition from the paleoclimatic transition from Pennsylvanian 'icehouse' to the Permian 'hothouse' conditions, and a host of other late Paleozoic problems will remain unresolved [6–11].

* Corresponding author. Tel.: +1 208 426 5907; fax: +1 208 426 4061.
E-mail address: markschmitz@boisestate.edu (M.D. Schmitz).

0012-821X/$ - see front matter © 2007 Elsevier B.V. All rights reserved.
doi:10.1016/j.epsl.2007.01.032

U–Pb dating of zircons from ash beds interstratified with fossiliferous strata has become an important means of calibrating the chronostratigraphic time scales derived by biostratigraphic zonation [12–14]. The geologically instantaneous nature of volcanic eruptions and the deposition of their eruptive products make even distal tuffs excellent event markers in the geological record. The U–Pb zircon technique is well suited to the dating of Paleozoic and older bentonites because of the particular resistance of zircon to alteration and recrystallization. This robust character extends even to the preservation of closed system U–Pb isotopic behavior within domains of single grains of zircon, thus fulfilling one of the fundamental tenets of an accurate geochronometer. When combined with the precision and accuracy inherent to isotope dilution measurements, ID-TIMS U–Pb zircon geochronology becomes the preferred method for determining the ages of Paleozoic bentonites and the calibration of chronostratigraphic time scales.

The Upper Paleozoic strata in the foreland of the southern Urals in Russia–Kazakhstan (Fig. 1) offer an unparalleled opportunity for accurate and precise time-scale calibration. Marine fossils are numerous and well preserved in this region, making detailed multi-taxa biostratigraphic control possible. Indeed, the southern Urals host the Global Stratotype Section and Point (GSSP) for the base of the Permian at Aidaralash Creek [15]. Additionally, the basinal Usolka (Krasnousolsk) section has been proposed as an auxiliary stratotype section to the GSSP for the Carboniferous–Permian boundary, in order to augment some features not present in the Aidaralash section [16,17]. Southern Urals stratigraphic sections are also candidates for the GSSPs of the rest of the middle-upper Pennsylvanian and lower Permian stages [1,18,19]. Thus, the internationally accepted biostratigraphic definition of the Pennsylvanian through Early Permian time scale is intimately linked to the region.

Volcanic-ash horizons are distributed throughout the southern Urals foreland, and form potentially important stratigraphic markers in the offshore facies of the Pennsylvanian–Early Permian of the Pre-Uralian Foredeep. Linking the available detailed biostratigraphic data to new precise radiometric ages (Fig. 2) in this region would significantly enhance the utility of the stratotype sections and reference sections as global standards.

2. Stratigraphic setting of the Carboniferous–Permian transition in the southern Urals

The Global Stratotype Section and Point (GSSP) for the base of the Permian (basal Asselian Stage) was

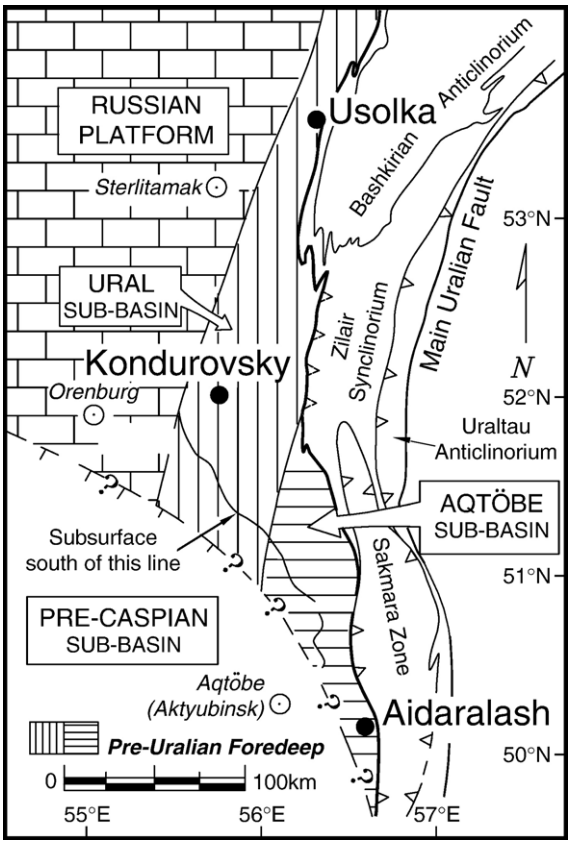

Fig. 1. Main elements of the southern Pre-Uralian foredeep, highlighting the position of the studied Usolka section relative to the GSSP for the Permo-Carboniferous boundary at Aidalarash.

ratified in 1996 by the International Union of Geological Sciences (IUGS) at Aidaralash Creek, Aktöbe (formerly Aktyubinsk) region, northern Kazakhstan [15]. The boundary is established at the first appearance of the conodont species *Streptognathodus isolatus* [16] within the *S. wabaunsensis–S. isolatus* conodont chronocline, 27 m above the base of Bed 19. The conodont succession observed at Aidaralash Creek is also displayed in other sections in the southern Urals including the basinal reference section at Usolka [20], in the Red Eagle cyclothem of the Mid-Continent of the United States [21], at the West Texas regional stratotype in the Wolfcamp Hills [18] and in China [22], and therefore serves as an excellent boundary definition.

The conodont succession in the Carboniferous–Permian boundary beds of the Usolka section is arguably represented in even greater detail than at Aidaralash Creek. The Carboniferous–Permian boundary at Usolka is precisely constrained within tens of centimeters: *S. wabaunsensis* ranges from 28.1 to 32.8 m above the base (mab) of the section (beds 16–1 through 16–4 [23,24]),

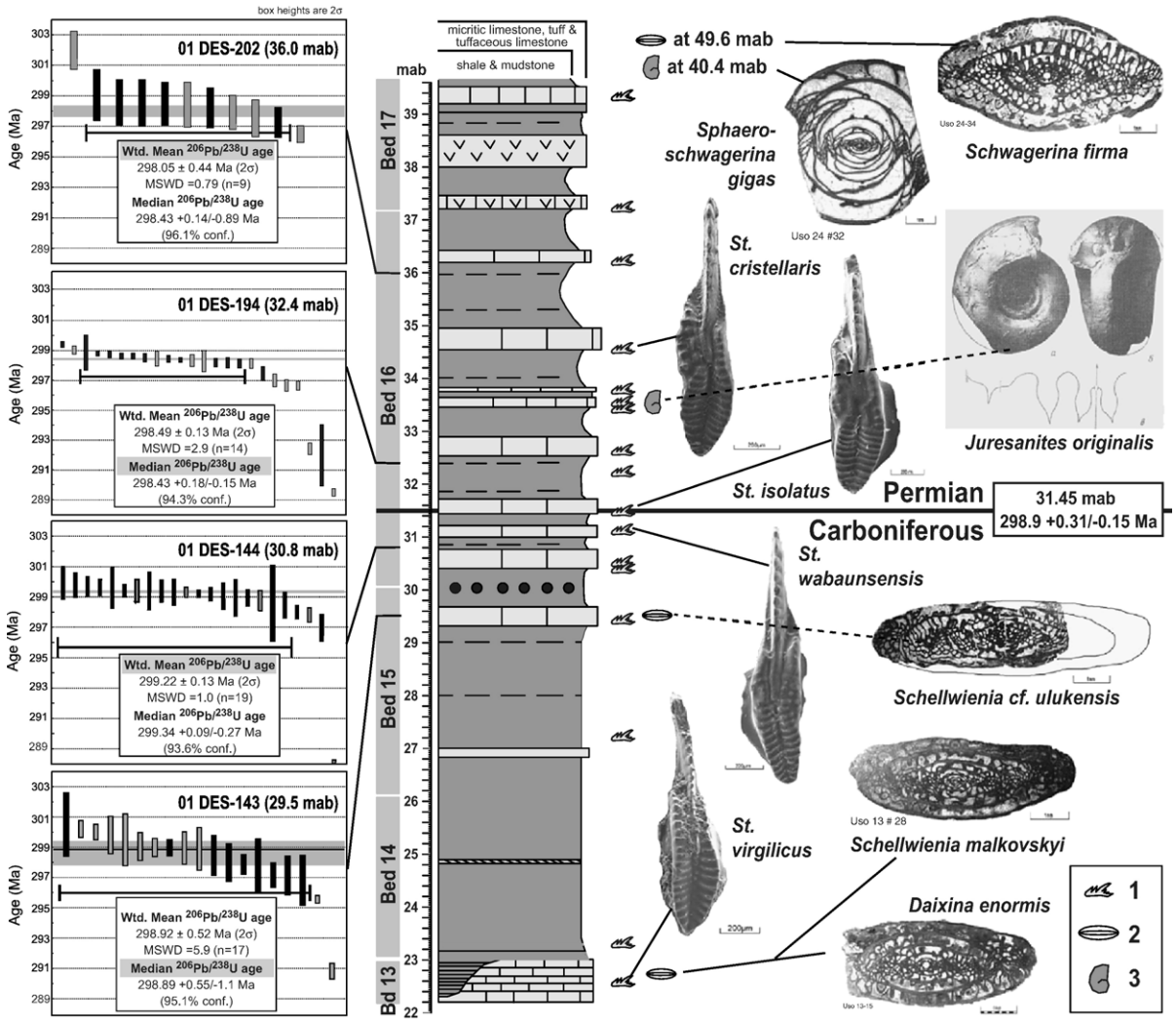

Fig. 2. Coupled biostratigraphic and ash bed U–Pb zircon geochronological data within the Carboniferous–Permian transition of the Usolka section. Bed numbers and biostratigraphic subdivision of the section are given according to [23,24] and our new data. Biostratigraphic data: 1 — conodonts; 2 — fusulinids; 3 — ammonoids. Ranked $^{206}Pb/^{238}U$ age plots: filled bars are annealed and chemically abraded single grains, open bars are physically-abraded single grains; horizontal bracket indicates analyses incorporated into age calculation.

and the first *S. isolatus* is found at 31.45 mab (bed 16–3). The ranges of other important species are shown in the Fig. 2; both fusulinid and ammonoid data support the position of the Carboniferous–Permian boundary constrained by conodonts [23,25,26].

Relevant to this study are more than 70 tuff layers that are distributed throughout the Kasimovian to Sakmarian stratigraphic interval in the Usolka section. The most probable volcanic source for the ash layers in the southern Pre-Uralian foredeep is the eastern part of the Tagil–Magnetogorsk arc, where Permian dikes and hypabyssal silicic and alkaline intrusions cut marine Visean through Moscovian sediments [27,28]. Preservation of volcanic ash in the southern Pre-Urals was strongly influenced by depositional environment; volcanic ash deposited in relatively deep-water environments such as those represented in the Usolka section (middle ramp, outer ramp, basin) had an apparent higher preservation potential than in shallower water depositional settings.

Most ash layers are easily recognized in the field because of their striking colors, including yellow-brown, red-brown and various shades of green. Their thickness varies from 1 to 5 cm. Both lower and upper contacts of volcanic-ash layers are sharp, generally planar, and can be clearly observed. The tuffaceous material is altered and poorly consolidated, erodes easily and outcrops recessively relative to the surrounding

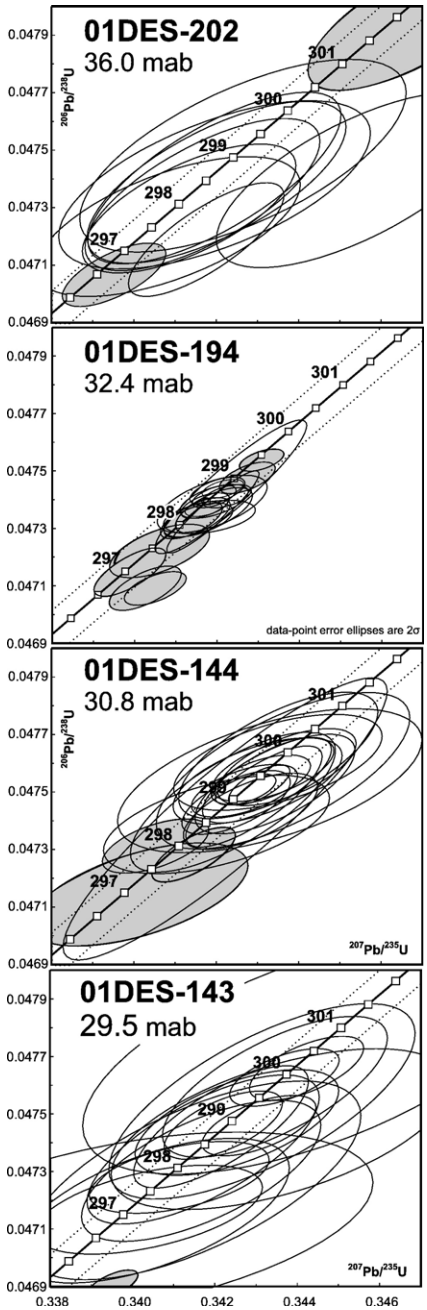

Fig. 3. Concordia plots for the analyzed ash bed single-zircon grains from the Carboniferous–Permian transition of the Usolka section. Dotted lines represent the uncertainties in the U decay constants. Analyses outside the plotted age range are not shown here.

clastic and carbonate strata. Most of the volcanic-ash layers have a distinctive soft, soapy texture. Four ash beds were sampled across the Carboniferous–Permian transition at Usolka for ID-TIMS U–Pb zircon geochronology (Fig. 2).

3. U–Pb geochronology

3.1. Analytical procedures

Zircons were concentrated from their altered bentonite matrix by emulsification, ultrasonication, and decanting of the clay fraction, followed by magnetic and heavy liquid separations. To minimize the effects of Pb loss, grains were pre-treated in one of two ways: removal of the outer parts of grains was accomplished by mechanical abrasion with pyrite inside air abrasion vessels [29]; or, the zircon grains were treated using a thermal annealing and partial dissolution technique (chemical abrasion or CA-TIMS) [30] designed to preferentially remove the high-U zones of the zircon crystal that are most susceptible to Pb loss. Zircons were annealed inside a furnace at 900 °C for 60 h, subsequently loaded into 200 μl PFA Teflon® microcapsules and leached in 29 M HF at 180 °C within high-pressure Parr® vessels for 12 h. The partially dissolved sample was then transferred into 3 ml Savillex® PFA beakers, fluxed successively with 4 M HNO_3 and 6 M HCl on a hot plate and in an ultrasonic bath, and rinsed with several millilitres of ultra-pure water in between fluxes. Air-abraded zircons were cleaned in a similar fashion by fluxing in warm 4 M HNO_3 in order to remove surface contaminants. After final rinsing of both air-abraded and annealed/leached zircons with ultra-pure water, zircon grains were loaded back into their microcapsules, spiked with a mixed ^{205}Pb–^{233}U–^{235}U tracer solution and dissolved completely in 29 M HF at 220 °C for 48–60 h. For one sample, 01DES-143, chemical abrasion was applied to the previously air-abraded zircon.

Dissolved Pb and U were chemically separated using a miniaturized HCl-based ion-exchange chromatography procedure modified after Krogh [31], using 50 μl columns of AG1x8 anion-exchange resin. The PFA dissolution vessels were cleaned in between analyses in four consecutive steps using concentrated HF and 6 M HCl solutions at dissolution temperatures over a period of four days. Both Pb and U were loaded with a silica gel–H_3PO_4 emitter solution [32] on single degassed Re filaments and their isotopic compositions measured on the VG Sector 54 multi-collector thermal ionization mass spectrometer at MIT. Lead isotopic measurements were made in a peak-switching mode by ion counting using a Daly photomultiplier detector with a ^{206}Pb ion beam intensity of 0.5 to 2.0×10^{-13} Amps usually maintained in the course of data acquisition. Uranium isotopes were measured as oxide ions on three Faraday detectors in a static mode with an average $^{235}U^{16}O_2^+$ ion

Table 1
U–Pb zircon data for ash beds from the Usolka section, Southern Urals, Russia

Sample fractions[a]	Composition			Ratios								Age (Ma)			
	Pbc (pg)[b]	Pb*/Pbc[b]	Th/U	$^{206}Pb/^{204}Pb$[c]	$^{208}Pb/^{206}Pb$[d]	$^{206}Pb/^{238}U$[e]	Err (2σ%)	$^{207}Pb/^{235}U$[e]	Err (2σ%)	$^{207}Pb/^{206}Pb$[e]	Err (2σ%)	Corr. coef.	$^{206}Pb/^{238}U$	$^{207}Pb/^{235}U$	$^{207}Pb/^{206}Pb$
01DES-202															
z8 aa	1.0	7.7	0.67	464.1	0.213	0.047960	(.43)	0.34686	(.62)	0.05245	(.43)	0.722	301.99	302.4	305.2
z18 ca	**0.4**	**6.1**	**0.92**	**352.1**	**0.291**	**0.047483**	**(.58)**	**0.34264**	**(.95)**	**0.05234**	**(.72)**	**0.654**	**299.05**	**299.2**	**300.1**
z15 ca	**0.8**	**7.1**	**1.14**	**384.6**	**0.362**	**0.047405**	**(.51)**	**0.34195**	**(.74)**	**0.05232**	**(.50)**	**0.730**	**298.57**	**298.6**	**299.3**
z11 ca	**1.0**	**6.4**	**0.79**	**372.3**	**0.271**	**0.047399**	**(.53)**	**0.34542**	**(.81)**	**0.05285**	**(.59)**	**0.683**	**298.54**	**301.3**	**322.5**
z17 ca	**0.3**	**7.8**	**1.00**	**432.8**	**0.319**	**0.047390**	**(.48)**	**0.34200**	**(.75)**	**0.05234**	**(.55)**	**0.685**	**298.48**	**298.7**	**300.3**
z9 aa	**0.6**	**6.9**	**0.94**	**392.2**	**0.299**	**0.047382**	**(.50)**	**0.34195**	**(.91)**	**0.05234**	**(.72)**	**0.612**	**298.43**	**298.6**	**300.4**
z13 ca	**0.6**	**8.3**	**0.94**	**470.5**	**0.299**	**0.047348**	**(.46)**	**0.34166**	**(.68)**	**0.05233**	**(.49)**	**0.701**	**298.22**	**298.4**	**300.1**
z2 aa	**0.3**	**10.8**	**0.88**	**610.0**	**0.282**	**0.047299**	**(.39)**	**0.34133**	**(.62)**	**0.05234**	**(.46)**	**0.665**	**297.92**	**298.2**	**300.2**
z4 aa	**0.3**	**9.4**	**1.15**	**503.0**	**0.368**	**0.047237**	**(.42)**	**0.34082**	**(.77)**	**0.05233**	**(.61)**	**0.604**	**297.54**	**297.8**	**299.8**
z14 ca	**1.0**	**13.2**	**1.17**	**692.3**	**0.382**	**0.047192**	**(.34)**	**0.34175**	**(.45)**	**0.05252**	**(.28)**	**0.777**	**297.26**	**298.5**	**308.2**
z3 aa	0.3	19.5	0.79	1113.9	0.252	0.047070	(.19)	0.33951	(.30)	0.05231	(.23)	0.669	296.51	296.8	299.1
01DES-194															
z9 aa	0.7	53.2	0.29	3421.0	0.092	0.064541	(.07)	0.48829	(.11)	0.05487	(.08)	0.681	403.18	403.7	406.9
z24 ca	0.2	70.8	0.52	4284.9	0.164	0.047537	(.07)	0.34308	(.13)	0.05234	(.11)	0.548	299.38	299.5	300.5
z8 aa	0.6	52.5	0.43	3253.8	0.136	0.047475	(.09)	0.34274	(.16)	0.05236	(.13)	0.611	299.00	299.2	301.1
z16 ca	**1.2**	**16.5**	**0.54**	**1007.1**	**0.170**	**0.047444**	**(.40)**	**0.34233**	**(.44)**	**0.05233**	**(.18)**	**0.918**	**298.81**	**298.9**	**299.9**
z27 ca	**0.2**	**94.2**	**0.53**	**5681.8**	**0.167**	**0.047437**	**(.06)**	**0.34215**	**(.12)**	**0.05231**	**(.10)**	**0.517**	**298.77**	**298.8**	**299.0**
z28 ca	**0.2**	**48.2**	**0.60**	**2862.5**	**0.191**	**0.047429**	**(.08)**	**0.34201**	**(.16)**	**0.05230**	**(.13)**	**0.564**	**298.72**	**298.7**	**298.5**
z26 ca	**0.2**	**68.2**	**0.48**	**4162.5**	**0.154**	**0.047411**	**(.07)**	**0.34223**	**(.14)**	**0.05235**	**(.12)**	**0.507**	**298.61**	**298.9**	**300.9**
z29 ca	**0.2**	**59.5**	**0.35**	**3774.9**	**0.110**	**0.047410**	**(.07)**	**0.34193**	**(.13)**	**0.05231**	**(.11)**	**0.558**	**298.60**	**298.6**	**298.9**
z23 ca	**0.2**	**37.3**	**0.61**	**2213.2**	**0.193**	**0.047394**	**(.10)**	**0.34193**	**(.20)**	**0.05233**	**(.17)**	**0.557**	**298.50**	**298.6**	**299.7**
z11 aa	**0.6**	**19.9**	**0.53**	**1211.2**	**0.169**	**0.047384**	**(.17)**	**0.34188**	**(.32)**	**0.05233**	**(.26)**	**0.595**	**298.44**	**298.6**	**299.8**
z30 ca	**0.2**	**51.6**	**0.41**	**3214.5**	**0.131**	**0.047379**	**(.08)**	**0.34171**	**(.14)**	**0.05231**	**(.12)**	**0.567**	**298.41**	**298.5**	**298.9**
z20 ca	**0.2**	**92.7**	**0.42**	**5751.7**	**0.133**	**0.047374**	**(.06)**	**0.34173**	**(.12)**	**0.05232**	**(.11)**	**0.494**	**298.38**	**298.5**	**299.3**
z6 aa	**0.8**	**27.5**	**0.59**	**1641.5**	**0.190**	**0.047362**	**(.14)**	**0.34192**	**(.22)**	**0.05236**	**(.17)**	**0.650**	**298.30**	**298.6**	**301.1**
z13 aa	**1.0**	**29.5**	**0.41**	**1847.2**	**0.132**	**0.047357**	**(.25)**	**0.34190**	**(.27)**	**0.05236**	**(.10)**	**0.926**	**298.27**	**298.6**	**301.2**
z19 ca	**0.4**	**50.7**	**0.51**	**3082.3**	**0.162**	**0.047339**	**(.10)**	**0.34182**	**(.27)**	**0.05237**	**(.24)**	**0.421**	**298.17**	**298.5**	**301.5**
z25 ca	**0.4**	**28.0**	**0.56**	**1688.6**	**0.178**	**0.047336**	**(.12)**	**0.34151**	**(.19)**	**0.05233**	**(.15)**	**0.656**	**298.15**	**298.3**	**299.7**
z22 ca	**0.5**	**47.8**	**0.60**	**2838.9**	**0.191**	**0.047329**	**(.10)**	**0.34154**	**(.20)**	**0.05234**	**(.17)**	**0.546**	**298.10**	**298.3**	**300.2**
z1 aa	0.6	38.5	0.67	2244.9	0.214	0.047328	(.11)	0.34138	(.18)	0.05231	(.14)	0.638	298.09	298.2	299.2
z21 ca	0.5	22.8	0.64	1351.5	0.203	0.047221	(.16)	0.34060	(.29)	0.05231	(.23)	0.594	297.43	297.6	299.1
z4 aa	1.0	22.3	0.44	1392.4	0.140	0.047147	(.15)	0.33988	(.21)	0.05228	(.14)	0.724	296.98	297.1	297.9
z5 aa	0.9	25.1	0.46	1548.7	0.148	0.047091	(.13)	0.34025	(.21)	0.05240	(.16)	0.653	296.63	297.4	303.1
z12 aa	0.6	38.4	0.46	2359.1	0.151	0.047090	(.10)	0.34049	(.18)	0.05244	(.14)	0.600	296.63	297.5	304.7
z3 aa	0.9	26.2	0.30	1684.8	0.098	0.046402	(.14)	0.33577	(.31)	0.05248	(.27)	0.502	292.39	294.0	306.5
z18 ca	0.6	4.5	0.66	276.4	0.213	0.046333	(.72)	0.33418	(1.20)	0.05231	(.91)	0.650	291.97	292.8	299.0
z10 aa	0.7	39.4	0.40	2454.8	0.134	0.045928	(.09)	0.33196	(.15)	0.05242	(.12)	0.623	289.48	291.1	303.8

z7 aa	0.7	35.7	0.46	2187.7	0.154	0.045576	(.10)	0.32997	(.16)	0.05251	(.12)	0.680	287.31	289.5	307.7
z2 aa	0.7	22.5	0.50	1360.2	0.174	0.044981	(.16)	0.32610	(.28)	0.05258	(.22)	0.622	283.64	286.6	310.7
01DES-144															
z5 aa	1.6	10.9	0.27	718.1	0.088	0.059051	(.46)	0.44317	(.70)	0.05443	(.49)	0.708	369.85	372.5	388.9
z24 ca	**0.3**	**8.5**	**0.59**	**520.3**	**0.185**	**0.047629**	**(.38)**	**0.34350**	**(.58)**	**0.05231**	**(.42)**	**0.682**	**299.95**	**299.8**	**298.8**
z25 ca	**0.2**	**11.0**	**0.47**	**690.0**	**0.148**	**0.047605**	**(.29)**	**0.34349**	**(.60)**	**0.05233**	**(.51)**	**0.546**	**299.80**	**299.8**	**299.9**
z21 ca	**0.3**	**14.5**	**0.61**	**869.3**	**0.195**	**0.047588**	**(.23)**	**0.34371**	**(.40)**	**0.05238**	**(.32)**	**0.614**	**299.70**	**300.0**	**302.2**
z22 ca	**0.3**	**16.4**	**0.50**	**1009.0**	**0.160**	**0.047580**	**(.19)**	**0.34337**	**(.35)**	**0.05234**	**(.28)**	**0.591**	**299.64**	**299.7**	**300.3**
z13 ca	**0.6**	**6.8**	**0.53**	**424.7**	**0.170**	**0.047576**	**(.47)**	**0.34361**	**(.73)**	**0.05238**	**(.54)**	**0.675**	**299.62**	**299.9**	**302.2**
z32 ca	**0.2**	**22.4**	**0.58**	**1348.6**	**0.184**	**0.047544**	**(.15)**	**0.34307**	**(.29)**	**0.05233**	**(.24)**	**0.566**	**299.43**	**299.5**	**300.1**
z6 aa	**0.5**	**14.3**	**0.53**	**873.9**	**0.169**	**0.047543**	**(.26)**	**0.34322**	**(.37)**	**0.05236**	**(.26)**	**0.718**	**299.42**	**299.6**	**301.1**
z29 ca	**0.3**	**7.3**	**0.45**	**464.4**	**0.145**	**0.047541**	**(.43)**	**0.34329**	**(.88)**	**0.05237**	**(.73)**	**0.563**	**299.41**	**299.7**	**301.6**
z30 ca	**0.3**	**12.3**	**0.55**	**752.2**	**0.176**	**0.047540**	**(.26)**	**0.34299**	**(.49)**	**0.05233**	**(.40)**	**0.586**	**299.40**	**299.4**	**299.8**
z14 ca	**0.6**	**11.0**	**0.51**	**679.1**	**0.165**	**0.047529**	**(.30)**	**0.34342**	**(.46)**	**0.05240**	**(.34)**	**0.675**	**299.34**	**299.8**	**303.1**
z27 ca	**0.2**	**39.6**	**0.45**	**2447.3**	**0.142**	**0.047511**	**(.09)**	**0.34270**	**(.17)**	**0.05231**	**(.14)**	**0.566**	**299.22**	**299.2**	**299.2**
z31 ca	**0.2**	**21.0**	**0.55**	**1271.6**	**0.174**	**0.047506**	**(.16)**	**0.34268**	**(.31)**	**0.05232**	**(.25)**	**0.572**	**299.19**	**299.2**	**299.2**
z4 aa	**0.4**	**54.3**	**0.58**	**3233.1**	**0.185**	**0.047526**	**(.12)**	**0.34303**	**(.18)**	**0.05235**	**(.13)**	**0.694**	**299.32**	**299.5**	**300.6**
z11 ca	**3.2**	**7.8**	**0.45**	**493.9**	**0.143**	**0.047486**	**(.30)**	**0.34291**	**(.39)**	**0.05237**	**(.24)**	**0.787**	**299.07**	**299.4**	**301.8**
z26 ca	**0.5**	**7.6**	**0.70**	**456.2**	**0.220**	**0.047466**	**(.42)**	**0.34239**	**(.59)**	**0.05232**	**(.40)**	**0.734**	**298.95**	**299.0**	**299.3**
z15 ca	**0.4**	**22.8**	**0.53**	**1389.0**	**0.167**	**0.047465**	**(.19)**	**0.34248**	**(.31)**	**0.05233**	**(.24)**	**0.641**	**298.94**	**299.0**	**299.8**
z1 aa	**0.8**	**14.5**	**0.50**	**896.9**	**0.160**	**0.047435**	**(.23)**	**0.34283**	**(.39)**	**0.05242**	**(.30)**	**0.628**	**298.76**	**299.3**	**303.6**
z12 ca	**1.8**	**8.6**	**0.37**	**560.1**	**0.117**	**0.047409**	**(.84)**	**0.34220**	**(.94)**	**0.05235**	**(.40)**	**0.905**	**298.59**	**298.8**	**300.8**
z17 ca	**0.7**	**11.0**	**0.53**	**676.3**	**0.169**	**0.047390**	**(.29)**	**0.34200**	**(.66)**	**0.05234**	**(.56)**	**0.531**	**298.48**	**298.7**	**300.3**
z16 ca	0.5	20.6	0.62	1228.2	0.194	0.047315	(.16)	0.34052	(.31)	0.05220	(.25)	0.580	298.02	297.6	294.0
z2 aa	0.7	22.1	0.55	1334.6	0.176	0.047284	(.16)	0.34144	(.24)	0.05237	(.17)	0.707	297.83	298.3	301.7
z18 ca	0.7	11.7	0.57	712.9	0.182	0.047146	(.31)	0.34012	(.64)	0.05232	(.53)	0.561	296.98	297.3	299.5
z7 aa	1.6	10.2	0.60	631.7	0.198	0.045587	(.33)	0.32908	(.54)	0.05236	(.41)	0.655	287.37	288.9	300.9
01DES-143															
z1 aa	0.5	7.4	0.18	452.3	0.174	0.046989	(.44)	0.44455	(.68)	0.06862	(.48)	0.707	296.01	373.5	887.2
z9 aa	0.5	18.1	0.55	1093.3	0.182	0.052005	(.20)	0.38261	(.33)	0.05336	(.25)	0.653	326.82	329.0	344.1
z16 ca	**1.0**	**4.4**	**0.53**	**281.2**	**0.169**	**0.047708**	**(.71)**	**0.34432**	**(1.32)**	**0.05234**	**(1.06)**	**0.597**	**300.43**	**300.4**	**300.5**
z10 aa	**0.4**	**19.1**	**0.53**	**1168.3**	**0.168**	**0.047660**	**(.19)**	**0.34422**	**(.33)**	**0.05238**	**(.26)**	**0.631**	**300.14**	**300.4**	**302.1**
z8 aa	**0.5**	**19.9**	**0.54**	**1209.7**	**0.170**	**0.047628**	**(.17)**	**0.34368**	**(.32)**	**0.05233**	**(.25)**	**0.599**	**299.94**	**300.0**	**300.1**
z6 aa	**0.6**	**7.5**	**0.51**	**468.8**	**0.161**	**0.047595**	**(.42)**	**0.34345**	**(.65)**	**0.05234**	**(.47)**	**0.690**	**299.74**	**299.8**	**300.1**
z7 aa	**1.4**	**5.5**	**0.61**	**344.1**	**0.192**	**0.047546**	**(.58)**	**0.34313**	**(.89)**	**0.05234**	**(.64)**	**0.696**	**299.44**	**299.5**	**300.3**
z11 aa	**0.5**	**10.9**	**0.58**	**662.7**	**0.183**	**0.047472**	**(.32)**	**0.34253**	**(.59)**	**0.05233**	**(.47)**	**0.598**	**298.98**	**299.1**	**299.9**
z13 aa	**0.6**	**16.2**	**0.52**	**994.9**	**0.164**	**0.047463**	**(.20)**	**0.34219**	**(.34)**	**0.05229**	**(.27)**	**0.633**	**298.93**	**298.8**	**298.1**
z3 aa	**0.4**	**20.2**	**0.38**	**1282.5**	**0.122**	**0.047461**	**(.18)**	**0.34306**	**(.33)**	**0.05242**	**(.26)**	**0.605**	**298.91**	**299.5**	**303.9**
z5 aa	**0.6**	**8.8**	**0.57**	**541.5**	**0.180**	**0.047457**	**(.36)**	**0.34214**	**(.51)**	**0.05229**	**(.34)**	**0.748**	**298.89**	**298.8**	**298.0**
z15 ca	**0.6**	**6.7**	**0.53**	**418.0**	**0.172**	**0.047449**	**(.48)**	**0.34360**	**(.98)**	**0.05252**	**(.82)**	**0.561**	**298.84**	**299.9**	**308.1**
z18 ca	**1.3**	**7.2**	**0.55**	**450.7**	**0.174**	**0.047378**	**(.45)**	**0.34170**	**(.68)**	**0.05231**	**(.48)**	**0.700**	**298.41**	**298.5**	**298.9**
z17 ca	**1.2**	**8.1**	**0.56**	**500.3**	**0.180**	**0.047304**	**(.42)**	**0.34165**	**(.70)**	**0.05238**	**(.53)**	**0.648**	**297.95**	**298.4**	**302.1**
z20 ca	**0.2**	**306.1**	**72.3**	**943.6**	**23.006**	**0.047282**	**(.22)**	**0.34112**	**(.52)**	**0.05232**	**(.46)**	**0.489**	**297.81**	**298.0**	**299.6**

(continued on next page)

Table 1 (*continued*)

Sample fractions[a]	Composition			Ratios								Age (Ma)			
	Pbc (pg)[b]	Pb*/Pbc[b]	Th/U	$^{206}Pb/^{204}Pb$[c]	$^{208}Pb/^{206}Pb$[d]	$^{206}Pb/^{238}U$[e]	Err (2σ%)	$^{207}Pb/^{235}U$[e]	Err (2σ%)	$^{207}Pb/^{206}Pb$[e]	Err (2σ%)	Corr. coef.	$^{206}Pb/^{238}U$	$^{207}Pb/^{235}U$	$^{207}Pb/^{206}Pb$
01DES-143															
z19 ca	**0.6**	**5.2**	**0.53**	**329.2**	**0.169**	**0.047271**	**(.60)**	**0.34146**	**(.98)**	**0.05239**	**(.74)**	**0.648**	**297.75**	**298.3**	**302.4**
z23 ca	**0.4**	**12.0**	**0.56**	**733.1**	**0.180**	**0.047169**	**(.27)**	**0.34038**	**(.66)**	**0.05234**	**(.58)**	**0.503**	**297.12**	**297.5**	**300.1**
z22 ca	**0.5**	**7.3**	**0.54**	**457.5**	**0.174**	**0.047166**	**(.43)**	**0.34046**	**(.80)**	**0.05235**	**(.65)**	**0.587**	**297.10**	**297.5**	**300.8**
z21 ca	**0.5**	**6.2**	**0.64**	**381.0**	**0.205**	**0.047116**	**(.56)**	**0.33977**	**(1.46)**	**0.05230**	**(1.30)**	**0.457**	**296.79**	**297.0**	**298.6**
z4 aa	0.5	43.7	0.56	2608.9	0.185	0.046910	(.09)	0.33951	(.15)	0.05249	(.11)	0.632	295.52	296.8	306.8
z2 aa	0.9	18.9	0.58	1129.0	0.192	0.046147	(.18)	0.33363	(.24)	0.05244	(.15)	0.767	290.82	292.3	304.4

Mass fractionation correction of 0.25%/amu±0.04%/amu (atomic mass unit) was applied to all single-collector Daly analyses.

Total procedural blank was less than 0.7 pg for Pb and less than 0.1 pg for U.

Blank isotopic composition: $^{206}Pb/^{204}Pb = 18.27 \pm 0.1$, $^{207}Pb/^{204}Pb = 15.59 \pm 0.1$, $^{208}Pb/^{204}Pb = 38.12 \pm 0.1$.

Corr. coef. = correlation coefficient $^{207}Pb/^{235}U$ and $^{206}Pb/^{238}U$ ratios.

Age calculations are based on the decay constants of Steiger and Jäger (1977).

Common-Pb corrections were calculated by using the model of Stacey and Kramers (1975) at 300 Ma.

[a] All analyses are single-zircon grains, those used in age calculations are in bold. aa = air-abraded, ca = annealed and chemically abraded.

[b] Pb_c is total common Pb in analysis. Pb* is radiogenic Pb concentration.

[c] Measured ratio corrected for spike and fractionation only.

[d] Radiogenic Pb ratio.

[e] Corrected for fractionation, spike, blank, and initial common Pb.

beam intensity of 8.0×10^{-13} amps. Measured isotopic ratios were corrected for mass-dependent isotope fractionation in the mass spectrometer, as well as for U and Pb contributions from the spike, laboratory blanks and initial Pb in the sample. Details of fractionation and blank corrections are given in Table 1.

3.2. Results

A total of 82 single zircon grains were analyzed from four volcanic-ash beds; data are reported in Table 1 and displayed in conventional concordia diagrams (Fig. 3). Fig. 2 illustrates the combined physical stratigraphy, biostratigraphic constraints, and ranked $^{206}Pb/^{238}U$ age plots for the Carboniferous–Permian transition in the Usolka section. Sample locations are reported as meters above the base of the stratigraphic section (mab).

Each ash bed in this study displays a zircon grain age distribution with variable scatter outside of analytical uncertainty, attributable to both discrete grain inheritance and varying degrees of Pb loss. Such age distributions are common to data sets obtained from bentonites [12–14]. Obvious inherited grains from the Usolka tuff samples are relatively rare and are distinctly older than the main zircon population. In contrast, Pb loss appears to be the major cause of scatter, with $^{206}Pb/^{238}U$ dates tailing off at the younger end of the main age clusters. Because this study was initiated before the adoption of the annealing and chemical abrasion (CA-TIMS) technique, data from each sample include a combination of physically-abraded grains and those treated by CA-TIMS. Following [30] and [13], we recognize the greater efficiency of the annealing and chemical abrasion method for mitigating Pb-loss phenomena, and thus have consistently relied upon such analyses in our age interpretations. However we have chosen not to simply discard all physically-abraded data, but rather to apply a consistent and objective filtering of data outliers prior to age calculation.

Our rationale for discarding outliers was two-fold and stepwise: first, outlying annealed and chemically abraded grain analyses (those with $^{206}Pb/^{238}U$ dates lying beyond the 2σ errors of the majority cluster of annealed and chemically abraded grains) were eliminated — by this criteria only two analyses from 01DES-144 and three analyses from sample 01DES-194 were discarded; second, all physically-abraded grain analyses with $^{206}Pb/^{238}U$ dates younger or older than the retained cluster of annealed and chemically abraded grains were discarded on the assumption that they are compromised by Pb loss (or in two cases, inheritance±Pb loss). Shaded ellipses on concordia diagrams illustrate those discarded analyses for each sample; on ranked $^{206}Pb/^{238}U$ plots, the error bars representing the calculated weighted mean $^{206}Pb/^{238}U$ and robust median $^{206}Pb/^{238}U$ ages span all included data.

We regard ages based upon zircon $^{206}Pb/^{238}U$ dates as the most accurate and reliable for the purpose of time-scale calibration, given that it has been demonstrated that high-precision zircon analyses are often characterized by a systematic discrepancy between $^{207}Pb/^{206}Pb$, $^{207}Pb/^{235}U$ and $^{206}Pb/^{238}U$ dates, which most likely stems from inaccuracies in one or both of the U decay constants [33,34]. Two calculated radiometric ages — the inverse-variance weighted mean $^{206}Pb/^{238}U$ age, and the median $^{206}Pb/^{238}U$ age (unweighted median age with asymmetric 95%-confidence errors) are reported and illustrated for each ash bed. Weighted mean age errors are herein reported at the 95% confidence interval (2σ) and are reported as $\pm Y(Z)$ Ma, where Y includes both analytical error and systematic MIT tracer calibration uncertainty [34] to allow for inter-laboratory comparison, and Z includes decay constant uncertainties, to facilitate inter-decay scheme comparison (e.g. comparisons to $^{40}Ar/^{39}Ar$ ages). The MSWD (mean squared weighted deviation) statistic testing data equivalence was calculated prior to the addition of systematic errors. When the MSWD of the weighted mean lies with its 95% confidence interval [35], indicating no excess geological scatter in the data, we have interpreted the weighted mean age as the depositional age of the tuff, otherwise the more robust (but generally less precise) median $^{206}Pb/^{238}U$ age with its asymmetric 95% confidence interval was thus interpreted.

3.2.1. Sample 01DES-202 (36.00 mab)

Sample 01DES-202 is a 2 cm thick ash bed located 4.55 m above the first appearance of *S. isolatus*. A total of eleven single-zircon grains were analyzed from this sample, of which one inherited analysis (z8) at 301.99 Ma and one analysis with apparent Pb loss (z3) at 296.51 Ma (both physically-abraded grains) were excluded from age calculation. The remaining nine analyses form a significant cluster with a weighted mean $^{206}Pb/^{238}U$ date of $298.05\pm0.44(0.54)$ Ma and an MSWD of 0.79 (Fig. 3). We interpret this as the age of deposition of the volcanic-ash bed. The median $^{206}Pb/^{238}U$ age of the same data cluster is $298.43^{+0.14}_{-0.89}$ Ma, which overlaps the weighted mean $^{206}Pb/^{238}U$ date well within uncertainties.

3.2.2. Sample 01DES-194 (32.40 mab)

Sample 01DES-194 is a 1 cm thick ash bed located 0.95 m above the first appearance of *S. isolatus*. Twenty-seven single-zircon analyses from this sample

range from 299.38 Ma to 283.64 Ma, with one obvious inherited analysis (z9) at 403.18 Ma. The distribution of dates (Fig. 3), however, points to both Pb loss and subtle inheritance at either end of the age spectrum. Discarding three outlying CA-TIMS and 10 physically-abraded grains according to the criteria stated above leaves a significant cluster of 11 CA-TIMS and 3 physically-abraded analyses with a weighted mean $^{206}Pb/^{238}U$ date of 298.49±0.13(0.34) Ma (MSWD=2.9). Due to the apparent excess scatter beyond analytical errors, we interpret the median $^{206}Pb/^{238}U$ age of 298.43+0.18/−0.15 Ma for the same data cluster as the time of tuff deposition.

3.2.3. Sample 01DES-144 (30.80 mab)

Sample 01DES-144 is a 4 cm thick ash bed located 0.65 m below the first appearance of *S. isolatus*. Of the twenty-four single-zircon grains analyzed from this sample, eighteen were treated using the CA-TIMS technique. Only one grain (z5) was demonstrably inherited with a discordant date of ca. 370 Ma. A pattern of Pb loss similar to that in sample 01DES-194 but to a more limited extent is observed in this sample. Excluding two outlying CA-TIMS and two physically-abraded grains leaves a group of nineteen analyses that form a significant cluster with a weighted mean $^{206}Pb/^{238}U$ date of 299.22±0.13(0.34) Ma (MSWD=1.0). We interpret this result as the age of tuff deposition, which directly places an upper limit on the age of the Carboniferous–Permian boundary. The median $^{206}Pb/^{238}U$ age is statistically identical at 299.34+0.09/−0.27 Ma.

3.2.4. Sample 01DES-143 (29.50 mab)

Sample 01DES-143 is a 1 cm thick ash bed located 1.95 m below the first appearance of *S. isolatus*. Due to the low yield of zircons from this tuff, the majority of grains were air abraded prior to development of the CA-TIMS method. All zircon crystals selected for analysis were thus drawn from the air-abraded pool. The first batch grains (z1–z11) were drawn from the highest quality air-abraded crystals, while the second batch of lower-quality air-abraded grains (z15–z23) were subsequently annealed and chemically abraded. The inferior quality of the second batch of grains is apparent in the analytical results, despite the annealing and chemical abrasion treatment. Nineteen zircon analyses, including nine treated by CA-TIMS, are characterized by a rather regular pattern of scatter (Figs. 2 and 3) from 300.43 Ma to 290.82 Ma (excluding two demonstrably inherited analysis at ca. 327 Ma and 890 Ma). This distribution renders any age interpretation prone to uncertainty. Discarding two physically-abraded grains at the young tail of the age spectrum, the remaining 17 analyses yield a weighted mean $^{206}Pb/^{238}U$ date of 298.92±0.52(0.61) Ma with a considerable scatter of data about the mean (MSWD=5.9). The median $^{206}Pb/^{238}U$ age is 298.89+0.55/−1.1 Ma, which we interpret as the deposition age of this tuff. While within error of the age for the overlying tuff at 30.8 mab (and thus confirming the age bracket on the Carboniferous–Permian boundary), the zircons of this sample appear to have retained a persistent amount of Pb loss even through the annealing and chemical abrasion treatment; recollection of high quality zircons and more vigorous treatments (higher temperatures and longer abrasion times) are warranted for future analyses of this sample.

4. Discussion

4.1. The global Permo-Carboniferous boundary

Our data represent the first high-resolution radiometric ages obtained from precisely located ash layers within the biostratigraphically-defined Carboniferous–Permian (C–P) boundary transition in the marine stratotypical sections of the southern Urals (Fig. 3), and thus represent a first step toward resolving significant global biostratigraphic and chronostratigraphic problems. In contrast to previous studies, we have provided a high-resolution (biostratigraphic and geochronologic) two-sided bracket on the boundary transition, from which we can calculate a precise radiometric age for the boundary. The boundary age is based upon a stratigraphically short interpolation between ash beds 01DES-194 and 01DES-144, assuming a constant sediment accumulation rate. It also incorporates stratigraphic error by estimating the age of the highest stratigraphic horizon in which *S. isolatus* is demonstrably absent (e.g. 31.0 mab), and adding the corresponding depositional time interval between these two biostratigraphic horizons to the older side of the boundary age confidence interval. Fortunately, the two ash beds bracket both of these biostratigraphic horizons, making this as robust an estimation of stratigraphic error as is possible. Our new age constraint on the C–P boundary is 298.90+0.31/−0.15 Ma (2σ), including both analytical error and stratigraphic uncertainty in the FAD. This new boundary age is immediately applicable to global marine sections through the detailed multi-taxa biostratigraphy of the southern Uralian sections [16,25,26]. We note that the error bounds on this age for the C–P boundary do not include uncertainty in the decay constant of ^{238}U, which is appropriate for comparison to a Paleozoic time scale constructed exclusively with $^{206}Pb/^{238}U$ ages. For intercomparison

with boundaries calibrated by other radiometric systems, e.g. $^{40}Ar/^{39}Ar$, the addition of ^{238}U decay constant uncertainty magnifies the boundary age error slightly, to 298.90+0.47/−0.34 Ma.

The commonly referenced ages for the C–P boundary are 290±20 Ma and 295±5 Ma based on estimates by Harland et al. [2] and Remane et al. [4], respectively. The recent time-scale revision of Davydov et al. [1] assigned a numeric age of 299±1 Ma to the C–P boundary based on preliminary reported results of this study [36]. Fig. 4 provides a summary of the isotopic ages available from various geographic regions, and highlights the prior lack of high-resolution radiometric age constraints for the C–P transition. The reliability of the estimated biostratigraphic position of the majority of geochronological samples above or below the boundary (denoted by stage abbreviations) also varies from region to region because of differences in local biostratigraphic control, the strong faunal and floral provincialism at this time, and difficulties in marine–terrestrial correlation. Consequently, several inconsistencies arising from either radiometric or stratigraphic uncertainties are apparent, and must be resolved by further high-precision biogeochronology.

Chuvashov et al. [37] were the first to report U–Pb SIMS (ion probe) zircon ages from the stratotypic Moscovian through Asselian of the southern Urals. One tuff horizon was collected in the Usolka section from bed 17 (lower middle Asselian, Fig. 3) and dated at 290.6±3.0 Ma. A tuff within the late Moscovian stage (uppermost Myachkovian substage) of another section along the Ural River was dated at 300.0±3.2 Ma. For comparative purposes, biostratigraphic control on the age in the Usolka section relative to our study is particularly good, with our dated ash bed 01DES-202 (298.05±0.43 Ma) located just 2.8 m below that of Chuvashov et al. [37]. Compared to our C–P boundary age of 298.90+0.31/−0.15 Ma, the results of Chuvashov et al. [37] appear significantly biased toward younger ages. Given the apparently robust biostratigraphic control, it is likely that these discrepancies resulted from analytical or interpretive bias in the U–Pb SIMS data. Thus we conclude that prior inference of the Carboniferous–Permian boundary at just slightly older than 290.6±3.0 Ma [38] is superseded by our new boundary age.

With regard to correlation to European successions, most of the continental Carboniferous–Permian stratigraphic sections of western Europe are correlated primarily based on fossil plants and palynomorphs. Although these taxa are widely used in the correlation of Upper Paleozoic strata, such correlations are often unreliable due to the endemism, environmental dependencies, or long ranges of such taxa. For example, the relationship between the classical European regional stages Stephanian C and Autunian remains poorly understood. It has been generally accepted that the

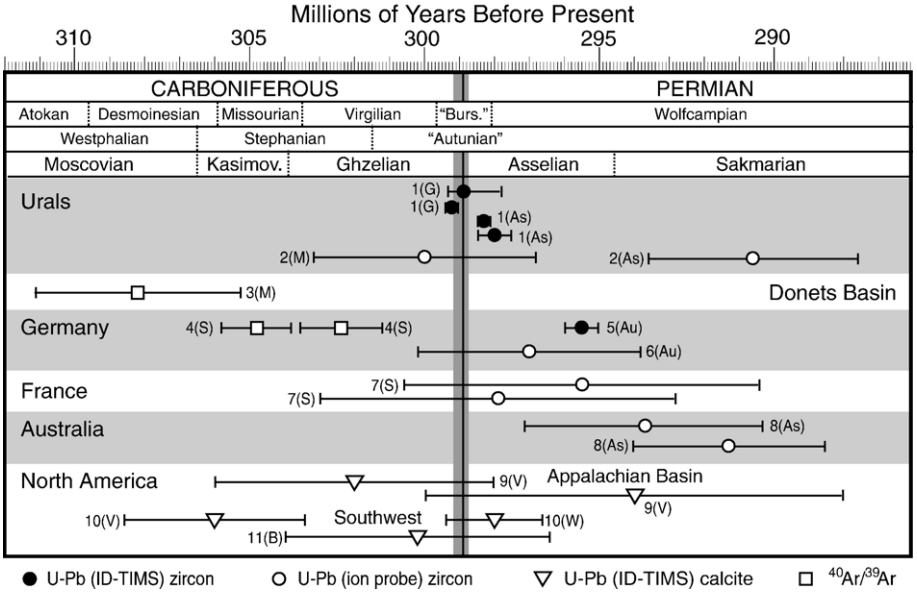

Fig. 4. Distribution of radiometric ages within the Carboniferous–Permian transition in different regions. Abbreviation after reference number indicates biostratigraphic provenance: As — Asselian; Au — Autunian; Bu/"Burs." — Bursumian; G — Ghzelian; M — Moscovian; S — Sakmarian; V — Virgilian; W — Wolfcampian. References: 1 — this study; 2 — [37]; 3 — [66]; 4 — [43]; 5 — [46]; 6 — [40]; 7 — [39]; 8 — [57]; 9 — [49]; 10 — [48]; 11 — [67].

Stephanian C is overlain by the Autunian. However, recently [39] obtained U–Pb SIMS zircon ages between 297.9±2.1 Ma and 295.3±4.8 Ma from the classical sections of the Stephanian C in the French Massif Central. At the same time, [40] obtained a virtually identical U–Pb SIMS age of 297.0±3.5 Ma from the basal Autunian in the Saar-Nahe Basin. Thus, either the uppermost Stephanian and lowermost Autunian are time-equivalent intervals [41,42] and therefore plant and palynomorph biostratigraphy should be considered with caution, or the U–Pb SIMS zircon ages from the Stephanian C and lower Autunian require major refinement.

Our new age for the Carboniferous–Permian boundary is, to first order, in better agreement with $^{40}Ar/^{39}Ar$ sanidine and ID-TIMS U–Pb zircon ages from the terrestrial successions of central Europe. Among these are sanidine $^{40}Ar/^{39}Ar$ plateau ages for the Saar Basin Tonstein 0 (Dilsburg Fm.) at 304.8±1.0 Ma, and the Baden-Baden tuff at 302.4±1.2 Ma [43] (all $^{40}Ar/^{39}Ar$ ages recalculated to the MMHb standard age of 523.1 Ma after [44]), which are biostratigraphically interpreted as Stephanian A and C respectively. The Stephanian C of central Europe is thought to correlate through the Donets Basin with the lower to middle Gzhelian of Eurasia [45]. In the Viala Formation, Lodéve, Franreich region, Germany, [46] obtained an ID-TIMS U–Pb zircon age of 295.5±0.5 Ma. This formation is placed in the uppermost Lower Rotliegendes and has been correlated with the upper Asselian Nikitovskaya and Slavyansjkaya Formations of the Donets Basin [45,47].

In North America, the method of U–Pb dating of caliche carbonates has been employed in chronostratigraphic studies of the upper Paleozoic cyclothemic successions in the Southwestern United States [48], and in the Appalachian basin [49]. Although this technique cannot achieve age precision comparable to the U–Pb zircon method, it can provide useful constraints in sections devoid of ash beds. In the Sacramento Mountains of New Mexico, calcite from a paleosol horizon six sedimentary cycles above the Missourian–Virgilian boundary has been dated at 306.0±2.6 Ma. In the subsurface eastern shelf of the Central Basin platform, part of the Midland Basin of West Texas, an approximately middle Wolfcampian paleosol horizon 22 cycles above the interpreted C–P boundary has been dated at 298.0±1.4 Ma [48]. However, the biostratigraphic age for this Wolfcampian soil horizon could be interpreted differently from that proposed in [48]. The fusulinids in the same interval of the UNOCAL Parker "X-1" well (*Eoparafusulina bispatula* Williams, *Schwagerina dispansa* Ross and *Schwagerina ex gr. neolata* Thomson) most likely indicate a Late Sakmarian or younger age [50], significantly above the C–P boundary. The same method used in the Appalachian region of North America provides U–Pb calcite ages of 302±4 Ma for the Late Desmoinesian and 294±6 Ma for the lower Virgilian [49], which appear too young according to currently held correlations between North American and Uralian stages [1,21]. We conclude that these U–Pb calcite ages must be considered with caution, as should estimated constraints on durations of Pennsylvanian cyclothems of the North American Mid-Continent that are based primarily on these ages [51,52]. We anticipate that more accurate constraints on cyclothem durations and definitive tests of cyclic drivers may be achieved through a combination of further high-precision radiometric age calibration in the Pennsylvanian of the southern Urals, and global biostratigraphic correlation to North America using cosmopolitan conodonts [21,53].

4.2. The timing of Permo-Carboniferous glaciations

The Permo-Carboniferous transition encapsulates major global paleoclimatic shifts attending the waning of the Gondwanan ice sheets [6,10,11]. Outstanding questions include the linkages between high-latitude glaciations of Gondwana and cyclothemic sedimentation across Euramerica [9,54]. However, correlation of Late Paleozoic paleoclimate proxies has been fundamentally limited by the lack of a coherent and precise age model for this time period. In particular, the biostratigraphic correlation of geologic events between the Euramerican and Gondwanan sectors of Pangaea is hampered by the zonal distribution and resulting provinciality of faunas across Pangaea, particularly in the low-diversity, high-latitude ecosystems of Gondwana [55,56].

Due to the limitations of biostratigraphic correlation, radiometric ages are particularly important for linking the records of Euramerica and Gondwana. Two Gondwanan data sets are available for comparison with the new constraint on the Permo-Carboniferous boundary. Roberts et al. [57] reported ages of 294±3 Ma and 291±3 Ma for volcanics of the New England orogen of Eastern Australia, which, when correlated paleontologically with the lowermost strata of the Sydney Basin, indicate a Early Sakmarian age for glaciation in Eastern Australia [56]. In southern Africa, Bangert and coworkers [58] dated tuff units in two deglacial sedimentary sequences of the Dwyka Group. The lower deglacial sequence (II) was dated by two ashes at 302±3 and 299±3 Ma, establishing a latest Pennsylvanian (mid-Ghzelian) age, while deglacial sequence III was dated by an

ash at 297±2 Ma. Importantly, this latter deglacial sequence is correlated with the Gondwana-wide *Eurydesma* transgression, which is thus dated as earliest Asselian by comparison with our new age for the Permo-Carboniferous boundary. Two tuffs in the overlying Prince Albert Formation of the Ecca Group were dated at 288±3 and 290±4 Ma, indicated that glaciation in southern Africa had terminated by the Early Sakmarian. While these new radiometric age constraints support earlier inferences of widespread Gondwanan ice-sheet formation in the Early Permian [59,60], they do suggest an asynchrony of glacial deposition between southern Africa and eastern Australia. These data also appear to exacerbate difficulties in correlating major glacial episodes in Gondwana with cyclothemic deposition on the Euramerican continental platforms throughout the Early and Middle Pennsylvanian [61–65].

5. Summary

The radiometric calibration of the base of the Permian is of profound importance, as it definitively establishes for stratal units of this relative age a same-time significance for geologists across the globe. This is true not just for stratigraphers, for whom a same-time equivalence is theoretically achieved through the definition of the GSSP, but also for the spectrum of tectonicists, petrologists, geochemists and geophysics who by necessity attempt to fuse stratigraphic and radiometric age constraints into holistic models of Earth evolution or process.

A precisely defined radiometric age for the Permo-Carboniferous boundary significantly stabilizes the Late Paleozoic time scale, and provides a prime reference point for global correlation between the Euramerican and Gondwanan sectors of Pangaea. Comparison with existing SHRIMP U–Pb zircon ages from tuffs in glacial strata of eastern Australia and southern Africa defines a major period of Gondwanan icehouse across the Permo-Carboniferous transition (latest Gzhelian through early Sakmarian), taking us a step closer to understanding the timing and tempo of glaciation and its far-field climatic and sedimentological effects.

Acknowledgments

This manuscript benefited from the constructive criticisms of two anonymous reviewers. We thank Dr. E.T. Rasbury for providing biostratigraphic data for the UNOCAL Parker X-1 well, and acknowledge support from NSF grants EAR-0003343, EAR-0106796, EAR-0418703, and EAR-0451802.

References

[1] V.I. Davydov, B.R. Wardlaw, F.M. Gradstein, The Carboniferous Period, in: F.M. Gradstein, J.G. Ogg, A.G. Smith (Eds.), A Geologic Time Scale 2004, Cambridge University Press, 2004, pp. 222–248.
[2] W.B. Harland, R.L. Armstrong, A.V. Cox, L.E. Craig, A.G. Smith, D.G. Smith, A Geologic Time Scale 1989, Cambridge University Press, 1990, 263 pp.
[3] F.M. Gradstein, J. Ogg, A Phanerozoic time scale, Episodes 19 (1996) 3–5.
[4] J. Remane, M.G. Bassett, J.W. Cowie, K.H. Gohrbandt, H.R. Lane, O. Michelsen, N. Wang, International Stratigraphic Chart with explanatory notes, Division of Earth Sciences, UNESCO, 2000, 16 pp.
[5] G.C. Young, J.R. Laurie, The Phanerozoic Timescale, in: L.J.R. Young (Ed.), An Australian Phanerozoic Timescale, Oxford University Press, Melbourne, 1996, pp. 6–11.
[6] T.J. Crowley, S.K. Baum, Modeling late Paleozoic glaciation, Geology 20 (1992) 507–510.
[7] R.A. Berner, Z. Kothavala, GEOCARB III; a revised model of atmospheric CO2 over Phanerozoic time, Am. J. Sci. 301 (2001) 182–204.
[8] A.J. Boucot, J. Gray, A critique of Phanerozoic climatic models involving changes in the CO2 content of the atmosphere, Earth-Sci. Rev. 56 (2001) 1–159.
[9] P.H. Heckel, Evaluation of evidence for glacio-eustatic control over marine Pennsylvanian cyclothems in North America and consideration of possible tectonic events, in: J.M. Dennison, F.R. Ettensohn (Eds.), Concepts in Sedimentology and Paleontology, vol. 4, 1994, pp. 65–87.
[10] J.T. Parrish, Climate of the supercontinent Pangea, J. Geol. 101 (1993) 215–233.
[11] C.R. Scotese, A.J. Boucot, W.S. McKerrow, Gondwanan palaeogeography and palaeoclimatology, J. Afr. Earth Sci. 28 (1999) 99–114.
[12] R.D. Tucker, T.E. Krogh, R.J. Ross Jr., S.H. Williams, Time-scale calibration by high-precision U–Pb zircon dating of interstratified volcanic ashes in the Ordovician and Lower Silurian stratotypes of Britain, Earth Planet. Sci. Lett. 100 (1990) 51–58.
[13] R. Mundil, K.R. Ludwig, I. Metcalfe, P.R. Renne, Age and timing of the end Permian mass extinctions: U/Pb geochronology on closed-system zircons, Science 305 (2004) 1760–1763.
[14] S.A. Bowring, D.H. Erwin, Y.G. Jin, M.W. Martin, K. Davidek, W. Wang, U/Pb zircon geochronology and tempo of the end-Permian mass extinction, Science 280 (1998) 1039–1045.
[15] V.I. Davydov, B.F. Glenister, C. Spinosa, S.M. Ritter, V.V. Chernykh, B.R. Wardlaw, W.S. Snyder, Proposal of Aidaralash as GSSP for base of the Permian System, Episodes 21 (1998) 11–18.
[16] V.V. Chernykh, S.M. Ritter, *Streptognathodos* (Conodonta) at the Carboniferous–Permian boundary stratotype section, Aidaralash Creek, Northern Kazakhstan, J. Paleontol. 71 (1997) 459–467.
[17] B.I. Chuvashov, V.V. Chernykh, M.F. Bogoslovskaya, Biostratigraphic characteristic of stage stratotypes of the Permian System, Stratigr. Geol. Correl. 10 (2002) 317–333.
[18] B.R. Wardlaw, V.I. Davydov, F.M. Gradstein, The Permian Period, in: F.M. Gradstein, J.G. Ogg, A.G. Smith (Eds.), A Geologic Time Scale 2004, Cambridge University Press, 2004, pp. 249–270.
[19] Y.G. Jin, B.F. Glenister, W.M. Furnish, G. Kotlyar, B.R. Wardlaw, H. Kozur, C. Ross, C. Spinosa, Revised operational scheme of Permian chronostratigraphy, Permophiles 25 (1994) 12–15.

[20] V.V. Chernykh, N.P. Reshetkova, The biostratigraphy and conodonts from Carboniferous–Permian boundary deposits on the west slope of the central and southern Urals, Uralian Branch, USSR Academy of Sciences, Sverdlovsk, 1987, [In Russian] 53 pp.
[21] S.M. Ritter, Upper Missourian–Lower Wolfcampian (Upper Kasimovian–Lower Asselian) conodont biostratigraphy of the Midcontinent, USA, J. Paleontol. 69 (1995) 1139–1154.
[22] C.Y. Wang, The base of the Permian System in China defined by *Streptognathodus isolatus*, Permophiles 36 (2000) 14–15.
[23] V.V. Chernykh, Zonal method in biostratigraphy: zonal conodont scale of the lower Permian in the Urals, Institute of Geology and Geochemistry, Uralian Branch of the Russian Academy of Sciences [In Russian], Ekaterinburg, 2005, 217 pp.
[24] B.I. Chuvashov, G.V. Djupina, G.A. Mizens, V.V. Chernykh, Krasnousolsk section, in: B.I. Chuvashov, A.E.M. Nairn (Eds.), Permian System: Guides to Geological Excursions in the Uralian Type Localities, Occasional Publications ESRI, New Series 10, University of South Carolina, Columbia, 1993, pp. 45–70.
[25] M.F. Bogoslovskaya, T.B. Leonova, A.A. Shkolin, The Carboniferous–Permian boundary and ammonoids from the Aidaralash section, southern Urals, J. Paleontol. 69 (1995) 288–301.
[26] V.I. Davydov, I.S. Barskov, M.F. Bogoslovskaya, E.Y.A. Leven, A.V. Popov, L.Z. Akhmetshina, R.I. Kozitskaya, The Carboniferous–Permian boundary in the former USSR and its correlation, Int. Geol. Rev. 34 (1992) 889–906.
[27] S.G. Chervyakovsky, First discovery of eruptive apparatus in the Magnotogorsk zone in the southern Urals, Annu. Inst. Geol. Geochem. (1978) 65–66.
[28] G.A. Mizens, Upper Paleozoic flysch of western Urals, Institute of Geology and Geochemistry, Uralian Branch, Russian Academy of Sciences, Sverdlovsk, 1997, 230 pp.
[29] T.E. Krogh, Improved accuracy of U–Pb zircon ages by the creation of more concordant systems using an air abrasion technique, Geochim. Cosmochim. Acta 46 (1982) 637–649.
[30] J.M. Mattinson, Zircon U–Pb chemical abrasion ("CA-TIMS") method: combined annealing and multi-step partial dissolution analysis for improved precision and accuracy of zircon ages, Chem. Geol. 220 (2005) 47–66.
[31] T.E. Krogh, A low contamination method for hydrothermal decomposition of zircon and extraction of U and Pb for isotopic age determination, Geochim. Cosmochim. Acta 37 (1973) 485–494.
[32] H. Gerstenberger, G. Haase, A highly effective emitter substance for mass spectrometric Pb isotope ratio determinations, Chem. Geol. 136 (1997) 309–312.
[33] J.M. Mattinson, Revising the "gold standard", the uranium decay constants of Jaffey et al., 1971, EOS, Trans. Am. Geophys. Union 81 (2000) S444.
[34] B.S. Schoene, J.C. Crowley, D.J. Condon, M.D. Schmitz, S.A. Bowring, Reassessing the uranium decay constants for geochronology using ID-TIMS U–Pb data, Geochim. Cosmochim. Acta 70 (2006) 426–445.
[35] I. Wendt, C. Carl, The statistical distribution of the mean squared weighted deviation, Chem. Geol. 86 (1991) 275–285.
[36] J. Ramezani, V.I. Davydov, C.J. Northrup, S.A. Bowring, B.I. Chuvashov, W.S. Snyder, Volcanic ashes in the Upper Paleozoic of the southern Urals: opportunities for high-precision calibration of the Upper Carboniferous–Cisuralian interval, Abstracts of the International Congress on Carboniferous and Permian Stratigraphy, 2003, pp. 431–432.
[37] B.I. Chuvashov, C.B. Foster, G.A. Mizens, J. Roberts, L.J.C. Claoue, Radiometric (SHRIMP) dates for some biostratigraphic horizons and event levels from the Russian and Eastern Australian Upper Carboniferous and Permian, Permophiles 28 (1996) 29–36.
[38] M. Menning, D. Weyer, G. Drozdzewski, H. van Amron, I. Wendt, A Carboniferous Time Scale: discussion and use of geological parameters as time indicators from Central and Western Europe, Geol. Jahrb. A156 (2000) 3–44.
[39] O. Bruguier, G.J.F. Bedq, M. Champenois, E. Deloule, J. Ludden, D. Mangin, Application of in situ zircon geochronology and accessory phase chemistry to constraining basin development during post-collisional extension: a case study from the French Massif Central, Chem. Geol. 201 (2003) 319–336.
[40] S. Königer, V. Lorenz, H. Stollhofen, R.A. Armstrong, Origin, age and stratigraphic significance of distal fallout ash tuffs from the Carboniferous–Permian continental Saar-Nahe Basin (SW Germany), Int. J. Earth Sci. (Geol. Rundsch.) 91 (2002) 341–356.
[41] J. Doubinger, Contribution a l'etude des flores autuno-stephaniennes, Mem. Soc. Geol. Fr. 75 (1956) 1–180.
[42] M. Menning, A numerical time scale for the Permian and Triassic periods: an integrated time analysis, in: P.A. Scholle, T.M. Peryt, D.S. Ulmer-Scholle (Eds.), The Permian of Northern Pangea, Springer-Verlag, Berlin, 1995, pp. 77–97.
[43] J.C. Hess, H.J. Lippolt, 40Ar/39Ar ages of tonstein and tuff sanidines: new calibration points for the improvement of the Upper Carboniferous time scale, Chem. Geol. 59 (1986) 143–154.
[44] P.R. Renne, C.C. Swisher, A.L. Deino, D.B. Karner, T.L. Owens, D.J. DePaolo, Intercalibration of standards, absolute ages and uncertainties in 40Ar/39Ar dating, Chem. Geol. 145 (1998) 117–152.
[45] V.I. Davydov, Zonal fusilinid subdivisions of Gzhelian in Donets Basin and Pre-Donets Trough, Problems of Modern Micropaleontology, Proceedings of the All-Union Paleontological Society 34, Nauka, Leningrad, 1990, pp. 52–69.
[46] E. Trapp, B. Kaufmann, Hochprazise U–Pb Datierungen von Pyroklastika im Jungpalaozoikum, Schwerpunktprogramm der duetschen Forschungsgemeinschaft DFG Spp, 1054, 2002, pp. 18–19.
[47] J.W. Schneider, Rotliegendstratigraphie — prinzipien und probleme, Beitr. Geol. Thuring. N.F. 8 (2001) 7–42 Jena.
[48] E.T. Rasbury, G.N. Hanson, W.J. Meyers, W.E. Holt, R.H. Goldstein, A.H. Saller, U–Pb dates of paleosols: constraints on late Paleozoic cycle durations and boundary ages, Geology 26 (1998) 403–406.
[49] M.L. Becker, E.T. Rasbury, G.N. Hanson, W.J. Meyers, Refinement in the age of the Carboniferous–Permian boundary based on U–Pb dating of biostratigraphically constrained synsedimentary carbonates in the Appalachian region of North America, Newsl. Carbonifer. Stratigr. 19 (2001) 18–20.
[50] V.I. Davydov, W.S. Snyder, C. Spinosa, Fusulineacean biostratigraphy of the Upper Paleozoic of the Southern Urals 27–30, 1997, pp. 31–34.
[51] P.H. Heckel, Observations and constraints on radiometric dating of the Pennsylvanian succession in North America and its correlation with dates from Europe, Newsl. Carbonifer. Stratigr. 20 (2002) 10–14.
[52] P.H. Heckel, Updated cyclothem constraints on radiometric dating of the Pennsylvanian succession in North America and its correlation with dates from Europe, Newsl. Carbonifer. Stratigr. 21 (2003) 12–20.
[53] D.R. Boardman II, M. Nestell, B.R. Wardlaw, Uppermost Carboniferous and lowermost Permian deposits and conodont

biostratigraphy of Kansas, USA, in: Y. Jin, B.R. Wardlaw, Y. Wang (Eds.), Permian Stratigraphy, Environments and Resources, Vol. 2, Stratigraphy and Environments, Paleoworld 9, 1998, pp. 19–32.
[54] T.J. Crowley, K.-J.J. Yip, S.K. Baum, Milankovitch cycles and Carboniferous climate, Geophys. Res. Lett. 20 (1993) 1175–1178.
[55] N.W. Archbold, G.A. Cisterna, T. Simanauskas, The Gondwana Carboniferous–Permian boundary revisited; new data from Australia and Argentina, Gondwana Res. 7 (2004) 125–133.
[56] N.W. Archbold, M. Dickins, J.M. Permian, in: G.C. Young, J.R. Laurie (Eds.), An Australian Phanerozoic Timescale, Oxford University Press, Oxford, 1996, pp. 127–135, (Chapter 6).
[57] J. Roberts, J.C. Claoue-Long, C.B. Foster, SHRIMP zircon dating of the Permian System of eastern Australia, Aust. J. Earth Sci. 43 (1996) 401–421.
[58] B. Bangert, H. Stollhofen, V. Lorenz, R. Armstrong, The geochronology and significance of ash-fall tuffs in the glaciogenic Carboniferous–Permian Dwyka Group of Namibia and South Africa, J. Afr. Earth Sci. 29 (1999) 33–49.
[59] J.C. Crowell, Pre-Mesozoic ice ages; their bearing on understanding the climate system, 1999, 106 pp.
[60] J.J. Veevers, M. Powell, Late Paleozoic glacial episodes in Gondwanaland reflected in transgressive–regressive depositional sequences in Euramerica, Geol. Soc. Amer. Bull. 98 (1987) 475–487.
[61] J.M. Dickins, Problems of a late Palaeozoic glaciation in Australia and subsequent climate in the Permian, Palaeogeogr. Palaeoclimatol. Palaeoecol. 125 (1996) 185–197.
[62] J.L. Isbell, P.A. Lenaker, R.A. Askin, M.F. Miller, L.E. Babcock, Reevaluation of the timing and extent of late Paleozoic glaciation in Gondwana; role of the Transantarctic Mountains, Geology 31 (2003) 977–980.
[63] J.L. Isbell, M.F. Miller, K.L. Wolfe, P.A. Lenaker, Timing of late Paleozoic glaciation in Gondwana; was glaciation responsible for the development of Northern Hemisphere cyclothems? Spec. Pap. - Geol. Soc. Am. 370 (2003) 5–24.
[64] A.T. Jones, C.R. Fielding, Sedimentological record of the late Paleozoic glaciation in Queensland, Australia, Geology 32 (2004) 153–156.
[65] G. Gonzalez-Bonorino, N. Eyles, Inverse relation between ice extent and the late Paleozoic glacial record of Gondwana, Geology 23 (1995) 1015–1018.
[66] J.C. Hess, H.J. Lippolt, K. Burger, High-precision 40Ar/39Ar spectrum dating on sanidine from the Donets Basin, Ukraine: evidence for correlation problems in the Upper Carboniferous, J. Geol. Soc. Lond. 156 (1999) 527–533.
[67] E.T. Rasbury, W.B. Ward, N.G. Hemming, H. Li, J.A.D. Dickson, G.N. Hanson, R.P. Major, Concurrent U–Pb age and seawater 87Sr/86Sr value of a marine cement, Earth Planet. Sci. Lett. 221 (2004) 355–371.